Physics of Fluids

Criterion for bubble encapsulation on drop impact onto a liquid film

Cite as: Phys. Fluids **35**, 033305 (2023); https://doi.org/10.1063/5.0138901
Submitted: 15 December 2022 • Accepted: 14 February 2023 • Published Online: 06 March 2023

D. Ribeiro, A. R. R. Silva and M. R. O. Panão

AIP Publishing

Physics of Fluids ARTICLE scitation.org/journal/phf

Criterion for bubble encapsulation on drop impact onto a liquid film

Cite as: Phys. Fluids **35**, 033305 (2023); doi: 10.1063/5.0138901
Submitted: 15 December 2022 · Accepted: 14 February 2023 ·
Published Online: 6 March 2023

D. Ribeiro,[1,a] A. R. R. Silva,[1,b] and M. R. O. Panão[2,c]

AFFILIATIONS

[1]AEROG—Aeronautics and Astronautics Research Center, LAETA, University of Beira Interior, Covilhã, Portugal
[2]ADAI—Associação para o Desenvolvimento da Aerodinâmica Industrial, LAETA, Department of Mechanical Engineering, Faculty of Sciences and Technology, University of Coimbra, Coimbra, Portugal

[a]Author to whom correspondence should be addressed: daniela.santo.ribeiro@ubi.pt
[b]Electronic mail: andre@ubi.pt
[c]Electronic mail: miguel.panao@dem.uc.pt

ABSTRACT

The phenomenon of bubble encapsulation results from droplet impact on a liquid film for specific impact conditions, but there is no established criterion for predicting its onset. Phenomenon visualization from two perspectives, the common lateral perspective and a bottom perspective, provided insights into the dynamics and formation mechanisms. Namely, the bottom shadowgraphs show capillary wavy patterns and perturbations imposed on the steady liquid film, which suggests a greater role of the liquid film in the onset of bubble encapsulation. Also, some considerations about the cavity development underneath the bubble limited by the solid wall allow concluding that the cavity shape is independent of the bubble encapsulation phenomenon. Additionally, using the bottom shadowgraphs, the crown closure time shows a systematic decrease in the dimensionless film thickness of $0.5 < \delta_f < 0.6$, which will be subject of future work. Finally, while most drop impact correlations focus on using the droplets' characteristics and thermophysical properties, the experimental results point in a different direction. Considering correlations relating the Ohnesorge and Reynolds numbers, the new criterion for the onset of bubble encapsulation uses drop characteristics and properties in the Reynolds number, while the liquid film thickness and thermophysical properties are used in the Ohnesorge number because most of the crown material comes from the liquid film. Therefore, the criterion based on 100% occurrence of bubble encapsulation is not a threshold, but a range: $k_{be} = ln(34.5/Re_D)/ln(Oh_f)$, with $k_{be} \in [1.022, 1.142]$. Other authors observed this phenomenon and despite being outside the validation range of this correlation, the values are close to their boundaries.

I. INTRODUCTION

The fundamental hydrodynamic and thermal-induced mechanisms of the single drop impact of size D_0 onto a liquid film of thickness h_f have been studied since the time of Worthington.[1] The most complex morphological event occurs when the impact energy is enough to form a liquid crown structure from which instabilities at the bounding rim lead to a secondary atomization process. Several authors identified the splashing phenomenology as prompt splash and crown splash.[2,3] However, for specific sets of impact conditions, prompt and crown splash are observed followed by the radial expansion of the crown liquid sheet, while the bounding rim remains fixed, leading to its inward closing and encapsulating a bubble that remains on the liquid film surface.[4] This bubble can burst by the impingement of secondary droplets that fall on top of the dome or by reaching a critical thickness due to the drainage of the liquid through the crown sheet walls.

Engel[5] related the crater of meteorite impacts with the impact of a liquid droplet onto a deep pool, and the morphology presented is similar to the observed for bubble encapsulation even in relatively thin liquid films ($0.2 < h_f/D_0 < 1$) as previously reported.[4] Engel[5] states that the impact energy of the impinging drop exceeds a minimum threshold, which is likely related to splash, and bubble formation attributed to a surface tension effect since the work of Worthington.[1] However, these works focused on the crater dynamics rather than the crown collapsing at the top and encapsulating a small bubble. Pan *et al.*[6] and Motzkus *et al.*[7] made a qualitative analysis of the bubble encapsulation. Pan *et al.*[6] claim that the transition boundary to obtain bubble encapsulation strongly depends on the dimensionless thickness of the liquid film ($\delta_f = h_f/D_0$). From a different perspective, Motzkus *et al.*[7] focused on the mechanisms of bubble bursting due to a lower hemispherical thickness of the dome by the rising bubble effect and

drainage of the liquid at the base. Geppert *et al.*[8] also observed the phenomenon and confirmed the boundaries for this event for dimensionless film thicknesses lower than the equivalent of a deep pool and within a certain range of impact Weber number ($1000 < \mathrm{We}_D = \rho U_0^2 D_0/\sigma < 1400$). However, none of these authors attempts to describe and explain the hydrodynamics of bubble encapsulation.

As mentioned, for deep pools, the crater dynamics is the main topic under research concerning the bubble encapsulation event.[1,5] However, in the case explored here, bubble entrapment occurs for droplet impact in thin liquid films and the crater is not spherical, but rather a half-disk with round edges because of the solid surface. It is important to emphasize that despite studies on moving liquid films have become more frequent,[9] this study is performed on steady liquid films. Therefore, in this work, one expects to retrieve insights into the hydrodynamics of bubble encapsulation by visualizing the phenomenon from below. Namely, what is the criterion for the onset of this event? What promotes this phenomenon? Can we relate this phenomenon with any existent correlations found in the literature? It is relevant to study this hydrodynamic phenomenon since the creation of bubble encapsulation needs to be avoided in applications involving spray painting. However, in applications involving spray cooling and fuel injection, the enlargement of the atomization process due to bubble bursting can be beneficial.

To answer these questions, this experimental study covers a wide range of impact conditions and two different visualization planes of the phenomenon. The overall purpose is to understand the dominant parameters in the formation and occurrence of bubble encapsulation to predict it.

II. EXPERIMENTAL TECHNIQUES

The conventional angle for visualizing drop impact dynamics is 90° from the normal to the impact surface, i.e., from the side. This viewpoint provides relevant information about the phenomena and the possibility of measuring and analyzing their features, e.g., crown height, diameter, angle, jet height, and number plus size of the secondary droplets. However, the lateral images do not allow a complete understanding of the phenomena, and other perspectives can also provide important knowledge.

In this study, one explores the viewpoints of single droplet impacts on thin liquid films from the side, and from below, with an experimental facility designed and built to acquire high-speed imaging of the phenomena. These two perspectives were acquired consecutively since we only have one high-speed digital camera.

Figure 1 shows a scheme of the experimental facility. The experimental setup consists of four main sections: image acquisition system, droplet dispensing system, liquid film container, and the illumination of the impact site. The main element in the image acquisition system is a high-speed digital camera Photron FASTCAM mini UX50 and a macro lens Tokina AT-X M100 AF PRO D. The camera has 1.3 Megapixel resolution at frame rates up to 2000 fps (frames per second) and up to 160 000 fps at reduced image resolution, and the lens has a focal length of 100 mm. The majority of the experiments were recorded at 2000 *fps*, but there are also some cases recorded at 4000 fps. The length scale resolution can vary between experiments, requiring proper calibration, but the average result was $34.6 \pm 0.2\,\mu$m/pixel. A medical syringe pump NE-1000 connected through medical tubes to a straight-tip stainless steel needle generates droplets at a pumping rate of 0.5 ml/min to minimize oscillation on the droplet after its release. It is possible to vary the impact velocity U_0 by changing the droplet falling height.

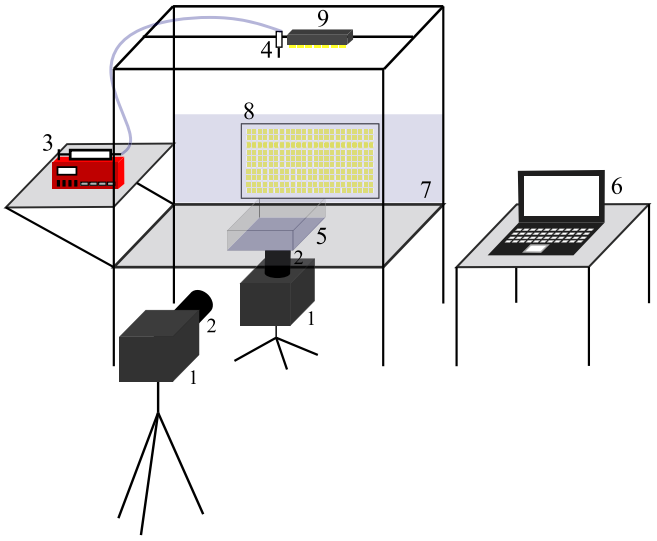

FIG. 1. Experimental setup: (1) high-speed digital camera, (2) macro lens, (3) syringe pump, (4) stainless steel needle, (5) liquid film container, (6) computer, (7) diffusion glass, and (8) and (9) set of LED's.

A topless right-angled perspex container accommodates the liquid film, and its size was calculated to ensure that the walls do not interfere with the phenomena. Its dimensions are 20×20 cm^2; consequently, the edge length is more than 60 times the maximum droplet initial diameter D_0. The liquid film thickness is produced by volume. Thus, the fluid volume necessary to have a specific thickness was inserted inside the container and confirmed using the high-speed digital camera. Producing such thin liquid films is challenging if the contact angle between the fluid and the surface is considerably high. However, in this case, the mixture with Jet A-1 and NExBTL shows a superhygrophilic behavior with the Perspex, which allows producing liquid films as thin as 100 μm. Ten experiments were performed for each set of experimental conditions. Due to a preliminary analysis, we concluded that ten droplets would not change the thickness of the liquid film by more than 1%. Therefore, the liquid film was remade after each set of 10 experiments. The thickness of the liquid film h_f is defined according to the droplet initial diameter D_0 to consider dimensionless film thicknesses $\delta_f = h_f/D_0$ between 0.1 and 1. Finally, the illumination of the impact site is vital to improve the quality of the images. A set of LEDs connected to a power supply was the only light source in the room. Also, a diffusion glass between the LEDs and the impact site ensured the uniformization of the backlight source for visualization purposes.

As shown in Fig. 1, the high-speed camera assumed two different positions to capture the droplet lateral impacting plane, and underneath the glass that supports the perspex container to capture images from below. Due to the glass transparency, the Perspex, and the liquid film, the camera captured the shadowgraph images of the drop impact from below using a light next to the needle working as a backlighting source.

TABLE I. Fluid thermophysical properties.

Substance	ρ (kg/m^3)	$\sigma \times 10^3$ (N/m)	$\mu \times 10^3$ (Pa s)
100% Jet A-1	798.3	25.4	1.12
75% Jet A-1–25% NExBTL	794.9	25.5	1.44

The phenomenon of bubble encapsulation was once again observed in the previous works[4,10,11] focused on the implementation of biofuels in civil aviation.[12] At this time, the legislation allows the use of fuel mixtures with at least 50% of the volume with conventional jet fuel.[13,14] Therefore, following the previous work,[10] the fuel mixtures used in the present experiments include a conventional jet fuel of 100% Jet A-1, a mixture with 75% of Jet A-1 and 25% of NExBTL (Neste Renewable Diesel), and a type of HVO (Hydroprocessed Vegetable Oil). The thermophysical properties of these fluids (density ρ, surface tension σ, and dynamic viscosity μ) were measured and are presented in Table I.

The droplet's initial diameter D_0 varied by changing the inner diameter of the dispensing needle ($2.6 < D_0 < 3.1$ mm). The impact velocity U_0 varied by changing the droplet falling height, providing impact velocities between 3.9 and 4.8 m/s. The usual dimensionless numbers that characterize the impact are the Weber number describing the ratio between the inertial and surface tension forces, $We_D = \rho U_0^2 D_0/\sigma$, and the Reynolds number as the ratio between the inertial and viscous forces, $Re_D = \rho U_0 D_0/\mu$. In this study, the Weber numbers varied between $1502 < We_D < 2180$ and the Reynolds numbers between $6263 < Re_D < 8358$, as shown in Table II, where all impact conditions that resulted in bubble encapsulation are detailed. Using this experimental facility and the impact conditions described above, the phenomenon of bubble encapsulation was observed both from the side and from below, and the perturbations imposed on the liquid film by the impact and crown collapse were analyzed.

III. VISUALIZATION AND ANALYSIS

In the first part of this section presenting and analyzing the visualization results, we explain in detail the phenomenology of bubble encapsulation (Sec. III A), show that cavity morphology is not a mandatory condition for the onset of this event, and provide evidence for the effect of the dimensionless film thickness on the crown closure time. Finally, we develop a criterion to predict the onset of this event following previous approaches for the splashing transition (Sec. III B).

A. Bubble encapsulation phenomenology

Bubble encapsulation is a complex phenomenon resulting from the closure of the crown upper rim in a splash event. The uprising sheet walls reach the maximum height in a relatively short timescale ($\tau = tU_0/D_0 < 5$), but the crown base still has enough radial momentum to grow into a diameter larger than its upper bounding rim. However, the hydrodynamic reason for keeping the upper rim in a fixed position can only be the supply of liquid through the vertical crown liquid sheet. As the rim thickens, surface tension forces lead to its collapse forming a bubble dome above the cavity, floating on the liquid film. Figure 2 shows a sequence of the first stages of impact from a bottom perspective, including illustrations of the lateral perspective. The white in the image implies the light is transmitted through a stagnated liquid film. Once the droplet approaches the film, and after its impact, the curvature reflects light and produces a shadow.[15] After impact, the fingering structures typical of a prompt splash are visible, and the thin white circular line sets the beginning of the kinematic discontinuity forming the uprising crown. The white spot in the first image results from the convergence of light at the top hemisphere of the impinging droplet, which works as a focal lens. This spot enlarges as not only the droplet mixes with the liquid film but

TABLE II. Parameter space.

Substance	Weber number We_D	Reynolds number Re_D	Dimensionless film thickness δ_f
100% Jet A-1	1565	8283	0.6, 1.0
	1593	8358	0.6, 1.0
75% Jet A-1–25% NExBTL	1502	6747	0.6, 1.0
	1503	6526	0.4, 0.6, 1.0
	1534	6817	0.6, 1.0
	1543	6263	0.4, 0.6
	1554	6637	0.4, 0.6, 0.8, 1.0
	1575	6327	0.6, 0.8
	1584	6345	0.8
	1587	6352	1.0
	1626	6429	1.0
	1650	6956	0.2, 0.3, 0.4, 0.5, 0.6, 0.7, 0.8, 0.9, 1.0
	1700	6943	0.8, 1.0
	1711	6594	0.4, 0.6, 0.8, 1.0
	1805	7395	0.4, 0.6, 0.8, 1.0
	1930	7396	0.4, 0.6, 0.8, 1.0
	2180	8127	0.6, 1.0

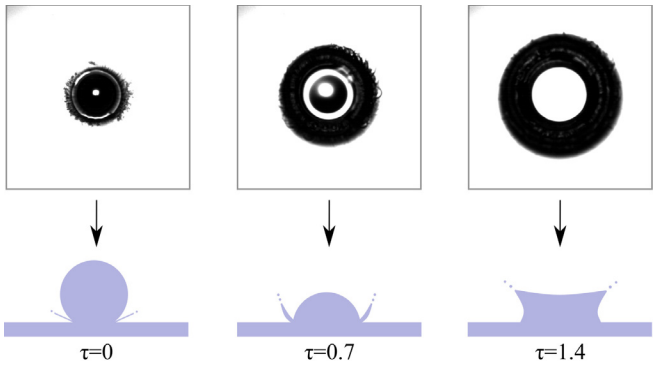

FIG. 2. First stages of the impact seen from the bottom perspective with schematics of the correspondent images from the lateral perspective. Length scale resolution 31.5 μm/pixel.

also the thin line thickens due to the inner curvature of the splashing uprising crown. The third image illustrates the complete immersion of the impinging droplet onto the liquid film forming a disk-shaped crater, and the shadow is proportional to the size of the perturbed liquid film forming the base that sustains the crown development.

The crown sheet height keeps increasing and capillary waves begin forming from the crown liquid sheet at its bottom.[16] For high-impact velocities and a combination of fluid thermophysical properties and dimensionless film thickness, the crown walls continue to expand at the base after the crown has reached its maximum height. This implies the timescale of crown formation is shorter than the timescale of the expansion of its base. In these conditions, the crown walls tend to bend inwards, as can be seen in Fig. 3(a) pointed by the arrow on the bottom perspective, and also in the top left image of Fig. 5. One of the advantages of this type of visualization is the possibility of determining the exact time of crown closure, which is difficult and inaccurate to define from the lateral perspective of the impact. Figure 3(b) shows the exact time when the crown rim merges to form a closed bubble above the liquid film. It is also possible to identify the shapes of capillary waves propagating on the bubble liquid sheet. There are also waves developing from the impact site to the undisturbed liquid film identified by the difference between black, gray, and white areas since the light transverse differently depending on if the curvature of the liquid film is concave or convex.

Previous studies[5,11] identified three different phenomenologies of bubble encapsulation. The example shown in Fig. 3 can be considered phenomenology 1, 2, or 3 since all of them involve the formation of a downward jet on the crown closure point. This jet is visible in the center of Fig. 3(c) by a darker circle with a white circle in the middle where the light at the top is fully transmitted to the bottom. Phenomenology 1 only has this downward jet, and phenomenology 2 has the formation of two jets, one upwards and other downwards. Finally, phenomenology 3 also has these two jets, but the upward jet is large enough to break and form a large secondary droplet. From the bottom images, it is not possible to conclude about the upward jet since it cannot be seen from this perspective. The perturbations imposed by the capillary waves, and also the fluid draining from the downward central jet, are visible by the different tones within the dome diameter since the interaction between light and the liquid films curvatures (bubble dome, liquid film) leads to the observed shadowy pattern. Finally, after a long period, these perturbations dissipate and both the horizontal liquid film and the bubble liquid sheet achieve a steady state, Fig. 3(d). Foltyn *et al.*[17,18] developed a study on single droplet impact upon smooth and micro-structured surfaces where they observed the phenomena from three different perspectives (lateral, bottom, and top). By using the bottom perspective and an air bubble that is entrapped at the droplet liquid film in the moment of impact, they used the LPSM method (LASER Pattern Shift Method) to measure the thickness of this liquid film.[19] In future works, this method should be considered in developing a new method to measure the thickness of the bubble liquid sheet.

Bubble lifetime further depends not only on small local instabilities but also on the impingement of tiny secondary droplets on the dome. Thus, when the bubble eventually bursts (see Fig. 4, $\tau = 344.4$), it induces several perturbations in the liquid film. Due to the burst of the bubble liquid sheet, tiny droplets formed with a size scaled by the thin liquid film of the bubble's dome impact the liquid and generate numerous perturbations (see Fig. 4, $\tau = 345.8$). The capillary waves generated by the impact of tiny secondary droplets propagate and interact with each other creating complex patterns, as visualized in the frames $\tau = 355.6$ and $\tau = 364$ of Fig. 4. From the bottom perspective, it is possible to observe the capillary waves' behavior and understand their evolution within and outside the area delimited by the preexisting bubble dome. In the study of Yu *et al.*,[20] it is also possible to observe these capillary waves but from a top perspective.

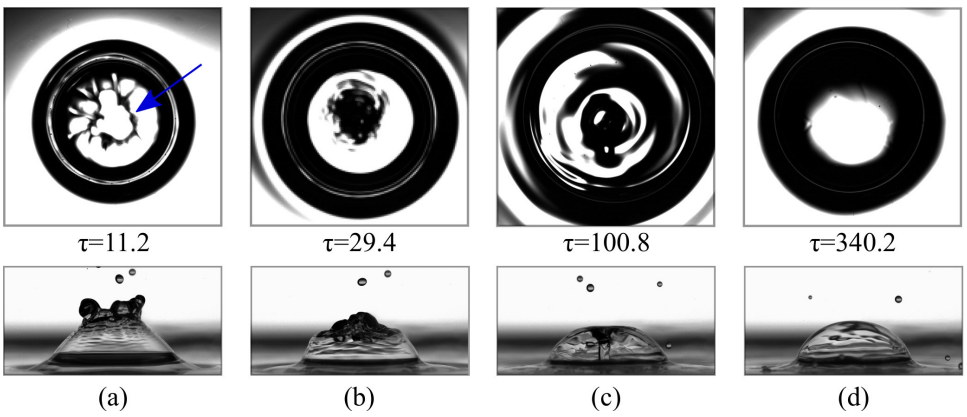

FIG. 3. Evolution of the perturbations imposed on the liquid film with bottom images on top and lateral images below: (a) crown liquid sheet bending inwards with the top of the crown pointed by a gray arrow, (b) crown sheet closure, (c) capillary waves propagating down the bubble liquid sheet and to the undisturbed liquid film, and (d) steady bubble liquid sheet on a steady liquid film. Length-scale resolution for the bottom images 31.5 and 37.1 μm/pixel for the lateral images.

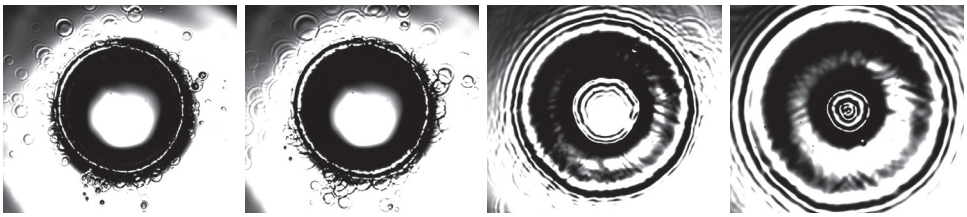

FIG. 4. Bubble bursting and propagation of capillary waves. Length-scale resolution 31.5 μm/pixel.

The cavity underneath the bubble has been a topic of extensive theoretical and experimental research.[1,5,6,21,22] However, in this work, visualization results confirm that bubble encapsulation is independent of the formation of a hemispherical crater. Instead, the cavity morphological development seems determined by the thickness of the liquid film with its own hydrodynamics. For deep pools, the cavity formed is usually hemispherical.[21] However, in the experiments reported here, the cavity touches the bottom of the container, as shown in Fig. 5. At first, while the crown sheet ascents, the cavity assumes a cylindrical shape and touches the bottom of the container. As the crown sheet wall bends and closes, the cavity becomes round at the sides but still touches the bottom. This shows that it is not necessary to have a fully developed cavity or a specific cavity shape to allow the formation of bubble encapsulation.

One of the benefits of the bottom images concerns the accurate determination of the crown closure time $t_{closure}$. From this perspective, it is clear when the jets at the top and the bounding rim close to form the spherical dome. For constant impact conditions at $We_D = 1650$ and $Re_D = 6956$, solely varying the dimensionless film thickness between $0.2 < \delta_f < 1.0$, Fig. 6 shows the crown closure time as a function of the liquid film dimensionless thickness. At $\delta_f = 0.5$, the crown closure time suddenly changes its trend, decreasing for $\delta_f = 0.6$ toward a nearly constant value around 12.5 ms. This change in the event's timescale is the subject of future research.

B. Onset of bubble encapsulation

Certain impact conditions always result in bubble encapsulation, meaning a probability of occurrence equal to unity, $p = 1$. However, there are also cases where $p < 1$. To calculate the probability of bubble encapsulation occurrence, 10 experiments were performed. For the range of impact conditions studied, considering several initial drop sizes expressed by the Ohnesorge number $Oh_D = \sqrt{We}/Re$, which relates the viscous to the inertial and surface tension forces, and the dimensionless film thicknesses, Fig. 7 shows how varying the impact energy (Re_D), a band appears associated with the emergence of bubble encapsulation. It means there are two transition boundaries: (1) a transition from splash to bubble encapsulation and (2) another transition returning to splash. Also, there is no evident effect of the liquid film thickness at the onset of bubble encapsulation.

Bubble encapsulation is a subsequent outcome after a splashing event triggered by a kinematic discontinuity at the boundary of the impinging droplet and the liquid film, meaning it depends on a combination of viscous, inertial, and surface tension forces. Therefore, we decided to compare these results with correlations available in the literature for the splashing threshold. In a previous review of spread/splash transition models, Ribeiro *et al.*[10] noted that the majority of the empirical correlations for this transition involving a constant coefficient K_c are in the form of

$$Re_D^{\alpha} We_D^{0.8} = K_c. \quad (1)$$

After analyzing the predictive value of different empirical correlations with experiments, Ribeiro *et al.*[10] showed the universal character

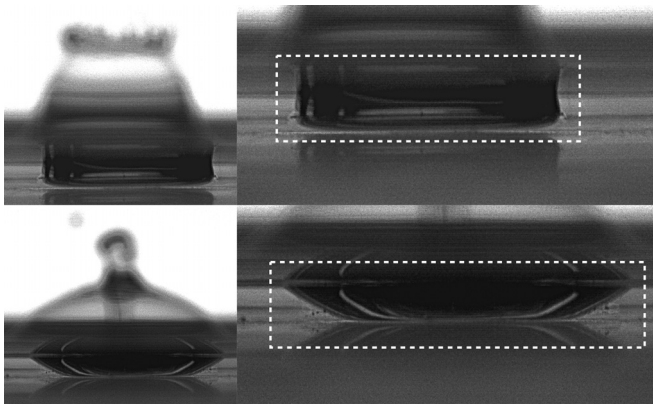

FIG. 5. Cavity shape during the crown sheet development (top) and during bubble encapsulation (bottom).

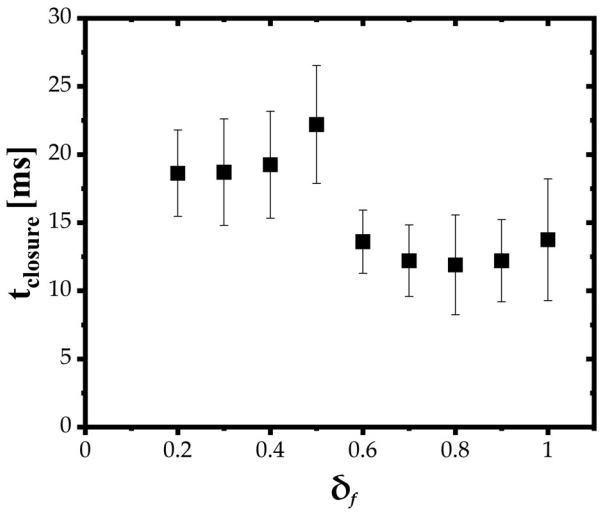

FIG. 6. Crown closure time depending on the dimensionless thickness of the liquid film.

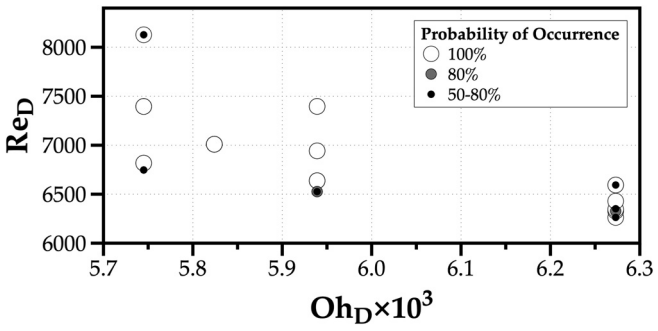

FIG. 7. Ohnesorge vs Reynolds map based on the initial drop size as length scale with the conditions resulting in 100%, 80%, and 50%–80% occurrence of bubble encapsulation.

of the criterion proposed by Vander Wal *et al.*,[23] which provided the best agreement with experimental data both within and outside its validation domain. The Vander Wal *et al.*[23] correlation is defined as

$$Re_D^{0.272} We_D^{0.8} = 756.7. \tag{2}$$

However, considering the Ohnesorge number relates all three forces involved in the morphology of bubble encapsulation, rearranging the correlation to include the Ohnesorge number, $Oh_D = \sqrt{We_D}/Re_D$, the general form of Eq. (1) becomes

$$Re_D Oh_D^a = K_c. \tag{3}$$

Considering this, the Vander Wal *et al.*[23] transition boundary becomes

$$Re_D Oh_D^{0.8547} = 34.5. \tag{4}$$

Figure 8 compares the Vander Wal *et al.*[23] correlation with our data (Re_D and Oh_D), considering the events of bubble encapsulation with different probabilities of occurrence. The black solid line represents the Vander Wal *et al.*[23] criterion from the transition between spreading and splashing after the droplet impact onto a liquid film, which does not depend on the dimensionless thickness of the liquid film. The white symbols describe the conditions where bubble encapsulation occurred for $p = 1$, the red middle-size ones for $p = 0.8$, and the blue smaller-size ones for $0.5 \leq p < 0.8$. The experimental results are within a region defined by the bottom (red line) and top (blue line) boundaries with the corresponding a and K_c values. The bottom boundary maintains the Vander Wal *et al.*[23] criterion, only changing the exponent a value, resulting in a transition parallel to the original correlation on a logarithmic scale. Regarding the top boundary, the transition was identified but does not follow the same trend, changing the values of a and K_c as $Re_D Oh_D^{2.2} = 0.1$.

However, the aforementioned analysis based on the Vander Wal *et al.*[23] correlation does not consider the influence of the liquid film thickness.

In several studies in the literature,[24–26] the material of the crown sheet formed after the impact of droplets onto liquid films is mainly composed of liquid from the film instead of the main droplet. This fact is relevant to our study. Therefore, instead of considering the Ohnesorge characteristic length as the initial drop diameter (Oh_D), we modified the Vander Wal *et al.*[23] transition boundary to consider the Ohnesorge number characteristic length scale based on the liquid film thickness h_f, Oh_f.

Figure 9 shows a clearer region where one can expect the occurrence of bubble encapsulation, with two limiting boundaries based on the Vander Wal *et al.*[23] correlation. These boundaries set the beginning of impact conditions that lead to bubble encapsulation (red line in Fig. 9) and when this phenomenon ceases to occur (blue line), meaning bubble encapsulation occurs for $1.022 < a < 1.142$. Since K_c value is constant for all equations, $K_c = 34.5$, one can develop a criterion for the onset of bubble encapsulation as

$$k_{be} = \ln(34.5/Re_D)/\ln(Oh_f), \quad \forall k_{be} \in [1.022, 1.142], \tag{5}$$

valid for $Re_D \in [6263; 8358]$ and $Oh_f \times 10^3 \in [4.776; 9.918]$. Other authors[6–8] obtain a bubble encapsulation for experiments outside the dimensionless film thickness validation range, where the experiments performed in this work had a probability of occurrence lower than 50% ($p < 0.5$). Figure 10 includes the validation domain of Eq. (5) and the values obtained for a outside this domain. The differences between

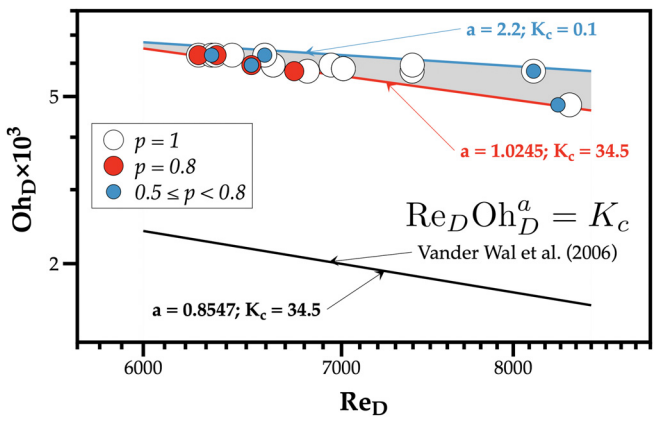

FIG. 8. Bubble encapsulation events compared with the spreading/splashing transition boundary of Vander Wal *et al.*[23]

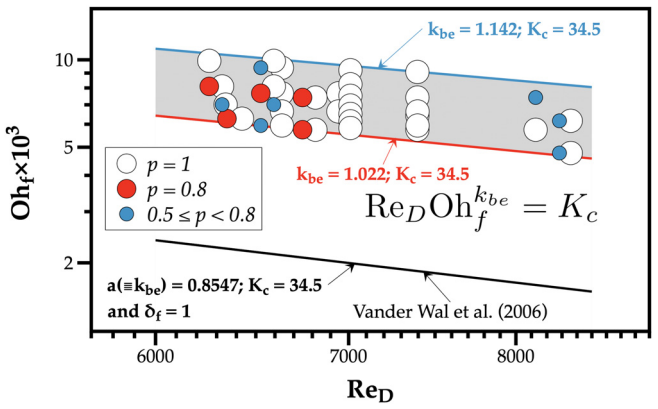

FIG. 9. Bubble encapsulation events compared with the spreading/splashing transition boundary of Vander Wal *et al.*[23] using the thickness of the liquid film h_f as the characteristic length scale in the calculation of the Ohnesorge number, Oh_f.

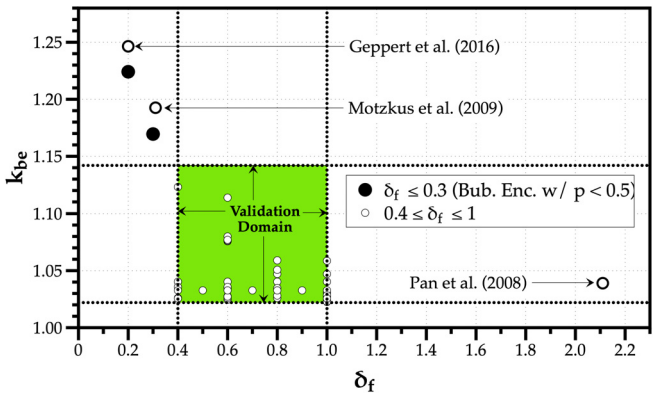

FIG. 10. Comparison with bubble encapsulation obtained by other authors and the present work when $p < 0.5$.

our values with $p < 0.5$ and the values of Geppert *et al.*[8] and Motzkus *et al.*[7] are lower than 2%, but the extension of the validation domain of the correlation would demand more experiments.

IV. CONCLUSIONS

Bubble encapsulation is a phenomenon occurring on a single droplet impact onto a liquid film in specific impact conditions. While there are criteria for the spread/splashing threshold, there is no criterion for the onset of bubble encapsulation. This work aims to provide a detailed morphology of the bubble encapsulation event from a bottom-view perspective and develop a criterion for its onset. Results evidence a region above the transition to splash threshold with 100% occurrence. However, there is no clear boundary considering that, in some cases, the phenomenon is observed with a lower probability of occurrence. The cavity created by these impacts was observed, and its shape does not influence the phenomenon since it touches the bottom of the container due to the small thickness of the liquid film. Moreover, with a bottom perspective, the capillary waves and perturbations observed were used to measure the crown closure time. Crown closure time depends on the dimensionless film thickness and shows an abrupt decrease between $\delta_f = 0.5$ and $\delta_f = 0.6$.

The occurrence of bubble encapsulation corresponds to a region above the spread/splashing transition. Therefore, based on the criterion proposed by Vander Wal *et al.*,[23] we propose a correlation based on the Ohnesorge number calculated using the thickness of the liquid film as the characteristic length scale and the Reynolds number based on the initial drop diameter as its characteristic scale, $k_{be} = \ln(34.5/\mathrm{Re}_D)/\ln(\mathrm{Oh}_f)$ with $k_{be} \in [1.022, 1.142]$, valid for $\mathrm{Re}_D \in [6263; 8358]$ and $\mathrm{Oh}_f \times 10^3 \in [4.776; 9.918]$. Future work includes experiments with heated liquid films to assess the validity of the correlation proposed and extend its validation domain.

ACKNOWLEDGMENTS

The authors would like to acknowledge the support of Fundação para a Ciência e a Tecnologia (FCT) through the Ph.D. scholarship No. SFRH/BD/140009/2018 and the Project No. UIDB/50022/2020. Miguel Oliveira Panão would like to acknowledge Project Nos. UIDB/50022/2020 and UIDP/50022/2020 of ADAI for the support provided for this publication.

AUTHOR DECLARATIONS

Conflict of Interest

The authors have no conflicts to disclose.

Author Contributions

Daniela Filipa Santo Ribeiro: Conceptualization (equal); Data curation (equal); Formal analysis (equal); Investigation (equal); Methodology (equal); Validation (equal); Visualization (equal); Writing – original draft (equal). **André Resende Rodrigues Silva:** Conceptualization (equal); Funding acquisition (equal); Investigation (equal); Project administration (equal); Resources (equal); Supervision (equal); Validation (equal); Writing – review & editing (equal). **Miguel Oliveira Panão:** Conceptualization (equal); Formal analysis (equal); Investigation (equal); Resources (equal); Supervision (equal); Validation (equal); Writing – review & editing (equal).

DATA AVAILABILITY

The data supporting this study's findings are available from the corresponding author upon reasonable request.

REFERENCES

[1]A. M. Worthington, *A Study of Splashes* (Longmans, Green, and Company, London, 1908).
[2]A. L. Yarin, I. V. Roisman, and C. Tropea, *Collision Phenomena in Liquids and Solids* (Cambridge University Press, Cambridge, 2017).
[3]G. Liang and I. Mudawar, "Review of mass and momentum interactions during drop impact on a liquid film," Int. J. Heat Mass Transfer **101**, 577–599 (2016).
[4]D. Ribeiro, M. Panão, A. Silva, and J. M. Barata, "Insights on bubbling formation after drop impact on thin liquid films," in *ILASS 2019-29th European Conference on Liquid Atomization and Spray Systems* (2019).
[5]O. G. Engel, "Crater depth in fluid impacts," J. Appl. Phys. **37**, 1798–1808 (1966).
[6]K.-L. Pan, K.-R. Cheng, P.-C. Chou, and C.-H. Wang, "Collision dynamics of high-speed droplets upon layers of variable thickness," Exp. Fluids **45**, 435–446 (2008).
[7]C. Motzkus, F. Gensdarmes, and E. Géhin, "Parameter study of microdroplet formation by impact of millimetre-size droplets onto a liquid film," J. Aerosol Sci. **40**, 680–692 (2009).
[8]A. Geppert, D. Chatzianagnostou, C. Meister, H. Gomaa, G. Lamanna, and B. Weigand, "Classification of impact morphology and splashing/deposition limit for n-hexadecane," Atomization Sprays **26**, 983 (2016).
[9]G. Gupta and P. Kumar, "Splashing dynamics of a drop impact onto a deep liquid pool with moving film interface," Phys. Fluids **32**, 012102 (2020).
[10]D. F. Ribeiro, A. R. Silva, and M. R. Panão, "Insights into single droplet impact models upon liquid films using alternative fuels for aero-engines," Appl. Sci. **10**, 6698 (2020).
[11]D. Ribeiro, M. O. Panao, J. M. Barata, and A. R. Silva, "Morphology of bubble formation on droplet impact upon thin liquid layers," AIAA Paper No. 2020-1577, 2020.
[12]I. Ferrão, D. Vasconcelos, D. Ribeiro, A. Silva, and J. Barata, "A study of droplet deformation: The effect of crossflow velocity on jet fuel and biofuel droplets impinging onto a dry smooth surface," Fuel **279**, 118321 (2020).
[13]ASTM D1655-19a, Standard specification for aviation turbine fuels, ASTM International, West Conshohocken, PA (2019).
[14]ASTM D7566-19b, Standard specification for aviation turbine fuel containing synthesized hydrocarbons, ASTM International, West Conshohocken, PA (2019).

[15]M. Selmke, "Bubble optics," Appl. Opt. **59**, 45–58 (2020).
[16]Y. D. Chashechkin, "Visualization of the fine perturbation structure of a liquid surface by flows induced by a drop impact," Fluid Dyn. **54**, 919–926 (2019).
[17]P. Foltyn, D. Ribeiro, A. Silva, G. Lamanna, and B. Weigand, "Influence of wetting behavior on the morphology of droplet impacts onto dry smooth surfaces," Phys. Fluids **33**, 063305 (2021).
[18]P. Foltyn, D. Ribeiro, A. Silva, G. Lamanna, and B. Weigand, "Influence of wetting behavior on the morphology of droplet impacts onto dry-patterned microstructured surfaces," Phys. Fluids **34**, 123322 (2022).
[19]P. Foltyn, L. K. Rihm, D. Ribeiro, A. Silva, and B. Weigand, "Measurement of the lamella thickness during droplet impact onto differently wettable smooth surfaces using an extension of the laser pattern shift method with naturally occurring patterns," Rev. Sci. Instrum. **92**, 105111 (2021).
[20]X. Yu, Y. Shao, K.-Y. Teh, and D. L. S. Hung, "Force of droplet impact on thin liquid films," Phys. Fluids **34**, 042111 (2022).
[21]A. Singh and P. Kumar, "Droplet impact dynamics onto a deep liquid pool of wavy free surface," Phys. Fluids **34**, 022107 (2022).
[22]T. Sun, H. Wang, Z. Zong, G. Zhang, A. Wang, and C. Xu, "Splash formation and cavity dynamics of sphere entry through a viscous liquid resting on the water," AIP Adv. **9**, 075211 (2019).
[23]R. L. Vander Wal, G. M. Berger, and S. D. Mozes, "The splash/non-splash boundary upon a dry surface and thin fluid film," Exp. Fluids **40**, 53–59 (2006).
[24]C. Josserand, P. Ray, and S. Zaleski, "Droplet impact on a thin liquid film: Anatomy of the splash," J. Fluid Mech. **802**, 775–805 (2016).
[25]A. B. Aljedaani, C. Wang, A. Jetly, and S. T. Thoroddsen, "Experiments on the breakup of drop-impact crowns by marangoni holes," J. Fluid Mech. **844**, 162–186 (2018).
[26]L. Lu, Y. Pei, J. Qin, Z. Peng, Y. Wang, and Q. Zhu, "Impingement behaviour of single ethanol droplet on a liquid film of glycerol solution," Fuel **276**, 117820 (2020).